Quantum Dephasing in a Gated GaAs Triple Quantum Dot due to Nonergodic Noise

M. R. Delbecq,[1,*] T. Nakajima,[1] P. Stano,[1,2] T. Otsuka,[1] S. Amaha,[1] J. Yoneda,[1] K. Takeda,[1] G. Allison,[1] A. Ludwig,[3]
A. D. Wieck,[3] and S. Tarucha[1,4]

[1]*Center for Emergent Matter Science, RIKEN, 2-1 Hirosawa, Wako-shi, Saitama 351-0198, Japan*
[2]*Institute of Physics, Slovak Academy of Sciences, 845 11 Bratislava, Slovakia*
[3]*Lehrstuhl für Angewandte Festkörperphysik, Ruhr-Universität Bochum, D-44780 Bochum, Germany*
[4]*Department of Applied Physics, University of Tokyo, 7-3-1 Hongo, Bunkyo-ku, Tokyo 113-8656, Japan*
(Received 2 December 2015; published 26 January 2016)

We extract the phase coherence of a qubit defined by singlet and triplet electronic states in a gated GaAs triple quantum dot, measuring on time scales much shorter than the decorrelation time of the environmental noise. In this nonergodic regime, we observe that the coherence is boosted and several dephasing times emerge, depending on how the phase stability is extracted. We elucidate their mutual relations, and demonstrate that they reflect the noise short-time dynamics.

Noise induces dephasing and loss of coherence of quantum systems. The finite resonance signal linewidth in the nuclear magnetic resonance (NMR) [1] or electron spin resonance (ESR) [2] experiment is one of its paradigmatic manifestations, allowing one to infer the corresponding dephasing time $T_2^\star$. As such experiments are usually performed in the steady state and on large ensembles of spins, this dephasing time reflects the system inhomogeneity over a large range both in space and time.

This dephasing is a central issue for further progress of quantum information science [3]. In electronic spin qubits realized in semiconductor quantum dots [4,5], the dominant noise is often the thermally fluctuating Overhauser field of nuclear spins [6,7]. The hallmark of this environment is its very slow internal dynamics [8], due to the weakness of nuclear spin-spin interactions [9,10]. This slowness allows strong suppression of the arising qubit dephasing by dynamical decoupling [11,12], or Hamiltonian estimation [13], techniques based on the ability to operate the qubit on times much shorter than the noise decorrelation time. This is a very different regime than that of the steady state NMR/ESR measurements, and one expects that the extracted dephasing might be strongly affected. We exploit the solid state qubit technology with its fast and sensitive readout techniques, to access dephasing in this regime. We investigate the nature of $T_2^\star$, which becomes a dynamical quantity itself, and its relation to the underlying noise dynamics.

We probe the coupled electron-nuclei system on time scales well below the nuclear spin decorrelation time, building on methods developed in Ref. [13]. Concerning nuclei, we find a striking subdiffusive behavior of the Overhauser field correlator, at odds with existing theories. Concerning the qubit, we demonstrate that the dephasing time depends sensitively on the way the coherence is measured. While in the ergodic regime the variance σ_B^2

of the Overhauser field B_N gives the qubit dephasing time as $1/(\pi\sqrt{2}\sigma_B)$, we find a larger phase coherence in the nonergodic regime. In addition, the phase coherence becomes a stochastic variable with a nontrivial probability distribution. Finally, working in the nonergodic regime of a diffusive noise, a tenfold decrease in the measurement time automatically prolongs the qubit phase coherence by roughly a factor of 3.

Our device is a triple spin qubit shown in Fig. 1(a). A micromagnet generates a magnetic field difference ΔB_{MM}^z between the dots [14]. Working between the (1,0,2) and (1,1,1) charge configurations, we manipulate the two rightmost dots as a singlet-triplet qubit [5,15] and leave
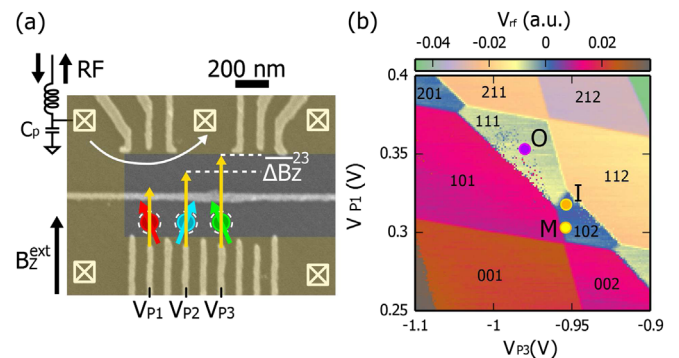

FIG. 1. (a) SEM micrograph of a similar device to the one measured. Lateral gates defining quantum dots (bottom) and charge sensors (top) are shown in light grey on the dark grey surface of the GaAs substrate. The three leftmost quantum dots are formed and manipulated while the upper left charge sensor, connected to an rf-reflectometry circuit is used. The "C-shaped" light colored area denotes the micromagnet providing inhomogenous magnetic field. An external magnetic field $B_z^{ext} = 0.7$ T is applied. (b) Charge stability diagram in the plane defined by plunger gates P_1 and P_3. The positions for initialization (I), operation (O), and measurement (M) configurations are denoted.

the leftmost spin qubit idle [see Fig. 1(b)]. The oscillation frequency of the singlet-triplet qubit $f = |g|\mu_B \Delta B_z / 2\pi\hbar$ (throughout the article we convert ΔB_z to frequency with this formula using g factor $g = -0.44$) is set by the magnetic field gradient $\Delta B_z = \Delta B_{MM}^z + \Delta B_{nuc}^z$, thus subject to nuclear field fluctuations.

We extract the qubit dephasing time $T_2^\star$ from the free induction decay, organizing the measurement scheme into the following hierarchy. The basic unit is a "cycle" (index c) during which the qubit is initialized in the state $|\uparrow, S(0,2)\rangle$, then quickly moved to the $|\uparrow, S(1,1)\rangle$ state where it precesses with $|\uparrow, T_0(1,1)\rangle$ for the qubit evolution time τ_c before undergoing a Pauli spin blockade measurement deep in the (1,0,2) region [16]. The cycle duration is set to 15.192 μs independent of τ_c by adjusting the initialization time. The next level is a "record", which comprises 250 consecutive cycles with qubit evolution times increased by 4 ns steps, restarting each record from zero. A single record takes time $t_{rec} = 3.8$ ms $= 250 \times$ 15.192 μs to acquire, covering the qubit evolution for $\tau_c \in [0, 996]$ ns. Finally, we form a set $\mathcal{R}$ by selecting $N_\mathcal{R}$ records from all measured ones. We extract the projection of the qubit state on the $S - T_0$ axis of the Bloch sphere, $s(\tau_c)$, by averaging over data in $\mathcal{R}$, using $s(\tau_c) = \langle 2P_S(\tau_c) - 1 \rangle_\mathcal{R}$ with $P_S \in \{0,1\}$ the results of projective measurements of the singlet state. The simplest choice is to take $\mathcal{R}$ as a block of N consecutive records. The time to acquire such data is $\Delta t = N t_{rec}$, henceforth referred to as the *acquisition* time. We select $\mathcal{R}$ also in other ways, but it always contains such blocks of N consecutive records. It defines the acquisition time Δt as a natural parameter for dephasing rates.

Indeed, even though we are interested in the qubit evolution on times of the order of $T_2^\star$, the acquisition time needed to sample the continuous function $s(\tau_c)$ from binary data of projective measurements is typically orders of magnitude larger, as is clear from the above measurement description. Now, if the acquisition time Δt is so large that the values of the fluctuating Overhauser field $B_N(t)$ and $B_N(t + \Delta t)$ are uncorrelated, the measurement is in the ergodic regime and always yields the same dephasing time $T_{2,\infty}^\star$ [5–7]. Our measurement is in the opposite—nonergodic—regime, with the noise decorrelation time much larger than the acquisition time. Here, one generally expects longer coherence [13] and nontrivial signatures of the noise dynamics reflected in the obtained $T_2^\star$ value.

We first extract the time evolution of ΔB_z over 40 000 consecutive records spanning more than 2 min [Fig. 2(a)]. It fluctuates around a finite value of 30 MHz, set by the micromagnet, by ± 20 MHz due to nuclei. With our measurement sequence we can follow the nuclei dynamics down to the time t_{rec}. Namely, using a Bayesian estimation algorithm [13,17] on the data of a single record, we estimate the mean and variance of the qubit frequency as it evolved during that record. The correlator

$C_{\Delta B}(\Delta t) = \Delta B_{nuc}^z(t + \Delta t) - \Delta B_{nuc}^z(t)$, shown in Fig. 2(a), displays a clear Gaussian probability distribution which broadens as the acquisition time Δt increases. As shown in Fig. 2(b), its variance grows as $\sigma_B^2(\Delta t) = D(\Delta t)^\alpha$ over more than 3 orders of magnitude of time span, with $\alpha = 0.8$ and $D = 0.048$ MHz^2/ms$^{0.8}$. Though we do not reach such long times in our measurement, the growth has to saturate, at $\sigma_B^2(\infty)$, since the fluctuating Overhauser field is bounded. Taking a value $\sigma_B(\infty)$ corresponding to $T_2^\star = 10$ ns typical for dots comparable to ours [5], we can roughly estimate the nuclear decorrelation time as $(\sigma_B^2(\infty)/D)^{1/\alpha} \approx 107$ s. For GaAs, values from seconds to hours are reported, the large range being due to effects of doping, strain, and nanostructure confinement [8].

More interestingly, the exponent $\alpha < 1$ indicates a surprising subdiffusive behavior. This differs from the normal diffusion (corresponding to $\alpha = 1$ [18]) that is assumed [19] for dipole-dipole interactions that should dominate at times equal or larger than our t_{rec}, and superdiffusion expected for electron-mediated interactions which should dominate at much shorter times [20]. Non-Markovian nuclear dynamics could result in such subdiffusion [21]; it would, however, also imply a non-Gaussian noise correlator [22], at odds with our observations. Since it is difficult to infer the correlator functional form in the time domain from its noise power spectrum [23] if the latter is
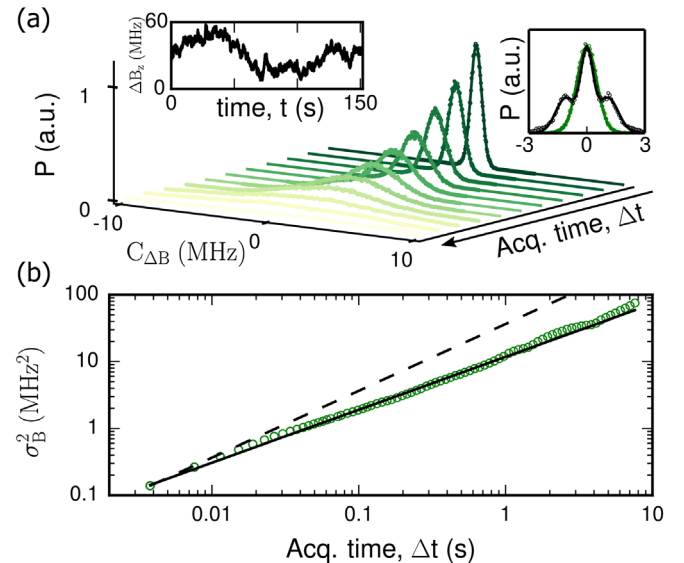

FIG. 2. (a) The probability distribution of the nuclear field gradient time correlator $C_{\Delta B}(\Delta t)$ for acquisition time Δt from 3.8 ms (dark green) to 7.6 s (yellow). Data (dots) are fitted with a Gaussian distribution (line). Left inset: Nuclear field gradient $\Delta B_z(t)$ extracted from the qubit frequency as a function of time. Right inset: correlator for $\Delta t = 3.8$ ms excluding (not excluding) the third spin fluctuation in green (black). (b) Variance of the nuclear field gradient correlator as a function of the acquisition time Δt. The solid line is a fit showing a growth with a power law exponent $\alpha = 0.8$. The dashed line shows a power law behavior with $\alpha = 1$ for comparison.

known only within a limited frequency range, previous investigations [24,25] do not necessarily contradict our observation. We also cannot completely exclude, due to our limited resolution, a behavior closer to standard diffusion at the shortest times we reach (Ref. [13] reports $\alpha = 1$ for times below 50 ms).

We now turn to the qubit phase stability. The standard way is to fit the qubit evolution to oscillations with a Gaussian decay

$$s(\tau_c) \xrightarrow{\text{fit}} \cos(2\pi f_0 \tau_c) \exp\left[-\left(\frac{\tau_c}{T_2^\star}\right)^2\right], \qquad (1)$$

and define the dephasing time as the fitted decay parameter. If τ_c is much smaller than the acquisition time, always fulfilled here, the frequency change during the time τ_c is negligible and we get

$$s(\tau_c) = \frac{1}{N_\mathcal{R}} \sum_{r \in \mathcal{R}} \cos\left(2\pi f_{c,r} \tau_c\right), \qquad (2)$$

with $f_{c,r}$ the qubit frequency during the cth cycle of the rth record. From here it follows that the frequency and dephasing extracted from the fit in Eq. (1) are given, respectively, as the average and the variance of the set of frequencies $\{f_{c,r}\}$. These statistical properties in turn depend on how the set $\mathcal{R}$ is chosen.

The standard way is to choose $\mathcal{R}$ as a single block of N consecutive records. Doing so we define $T_{2,\phi}^\star$, and observe a gradual increase of $T_{2,\phi}^\star \sim 120$, 220, and 570 ns upon decreasing N, for acquisition times $\Delta t \sim 1.6$, 0.4, and 0.1 s; see Fig. 3(a). Since each of these qubit evolutions results from a particular noise realization, $T_2^\star$ becomes a stochastic variable itself. We are able to extract its probability distribution for various acquisition times, as shown in Fig. 3(b). It is always well fitted by a Gamma distribution [26] whose skewness does not significantly change for Δt
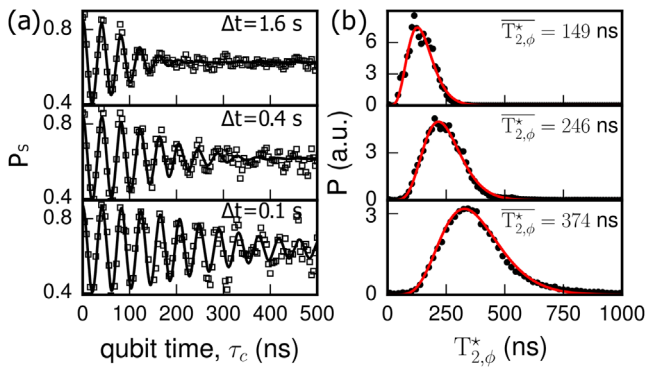

FIG. 3. (a) Typical qubit evolution traces for different acquisition times. Solid lines are fit to decaying oscillations, giving $T_{2,\phi}^\star = 120$, 220, and 570 ns, respectively. (b) Probability density distributions of $T_{2,\phi}^\star$ corresponding to the same acquisition times as for (a). The red solid line is a fit to a Gamma distribution resulting in skewness $\gamma_1 \approx 0.75$, and $\overline{T_{2,\phi}^\star} \approx$ as given.

varying from 38 ms to 7.6 s. We interpret this robustness as a signature that the nature of the underlying dynamics of nuclei does not change within this time span. We conclude that a single trace is not sufficient to reliably estimate the phase decay, as the most probable $T_{2,\phi}^\star$ is smaller than the mean $\overline{T_{2,\phi}^\star}$, whereas occurrences of $T_{2,\phi}^\star$ several times larger than $\overline{T_{2,\phi}^\star}$ are common.

This method is limited by the inherent noise of the quantum mechanical projective measurement and readout errors, the impacts of which increase as $N_\mathcal{R}$ decreases. We find that a minimum of ten records is required to get a reliable $\overline{T_{2,\phi}^\star}$. To access dephasing below this limit, we use a postselection method; see the top inset of Fig. 4(a). We include in $\mathcal{R}$ all blocks of N consecutive records for which the Bayesian estimated frequency of the first one is within $f_0 \pm \Delta f/2$ (upward red arrows). For example, choosing $f_0 = 20$ MHz and $\Delta f = 0.1$ MHz gives 167 such blocks, resulting for $N = 1$ in the red trace shown in the lower inset of Fig. 4(a), giving a coherence time $T_{2,ps}^\star \sim 3$ μs. Strikingly, we observe a beating pattern with frequency $\delta f \approx 1.16$ MHz. Both the beating frequency and amplitude are consistent with thermal flips of the tunnel coupled spin in the leftmost dot, which lead to discrete jumps of the qubit oscillation frequency [26]. The beating could only be unraveled thanks to the long coherence time we reach.

The dephasing times described above demonstrate a significant improvement compared to the 10 ns observed in the ergodic regime, but they cannot be taken as the measure of phase stability for general quantum computation (QC) algorithms. Indeed, the qubit oscillation frequency f_0 is only known after the fit in Eq. (1) is performed, and therefore the measurement is finished, limiting its practical use for postprocessing or echo techniques [15,27,28]. To access the dephasing time of a qubit whose frequency is known in advance [13], which we denote as $T_{2,QC}^\star$, we select blocks by beginning with the records *following* those with frequency $f_0 \pm \Delta f$ [downward purple arrows in the inset of Fig. 4(a)]. This set $\mathcal{R}$ can be thus obtained from the one in the previous paragraph by shifting all the records' indexes by 1. The resulting trace is shown in purple in the lower inset of Fig. 4(a) with $T_{2,QC}^\star \sim 600$ ns. The comparison of the different dephasing times is summarized on Fig. 4(a) as a function of the acquisition time. We also include the nuclear field correlator variance through $T_{2,B}^\star(\Delta t) = 1/[\pi\sqrt{2}\sigma_B(\Delta t)]$, the relation valid in the ergodic regime.

The relations between these quantities are governed by the nuclear field dynamics. Approximating the nuclear dynamics as a random walk ($\alpha = 1$), we were able to derive the following analytical results, valid for large N, hence long acquisition times, but still in the nonergodic regime (see Ref. [26] for details). First,

$$\frac{\overline{T_{2,\phi}^\star}}{T_{2,B}^\star} = \sqrt{6} \frac{k}{\sqrt{(k-1)(k-2)}} \approx 3, \qquad (3)$$
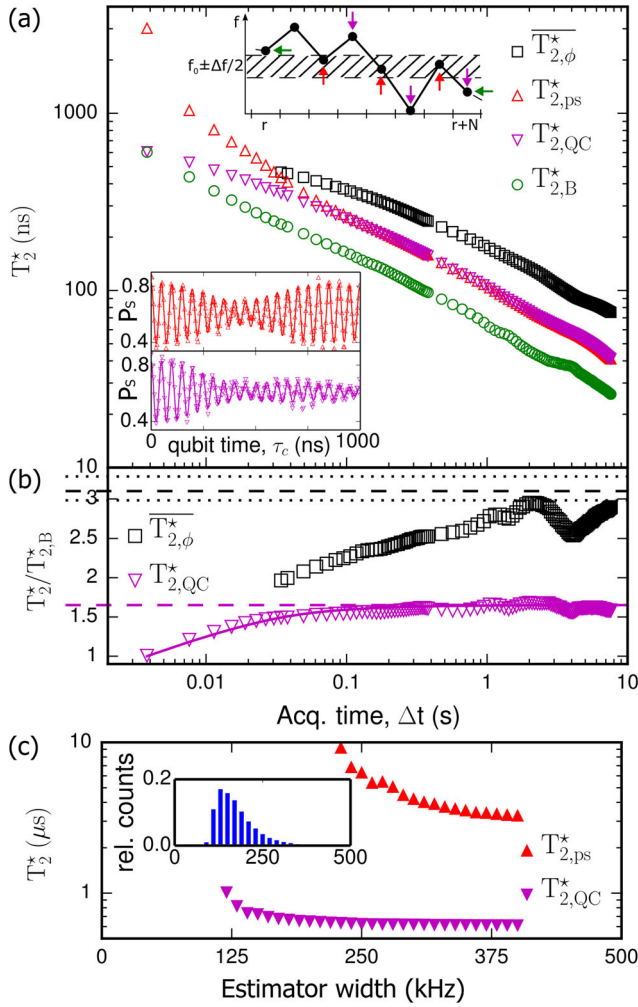
FIG. 4. (a) $T_2^\star$ from the different processings as a function of acquisition time Δt. Top inset: estimated frequencies of eight consecutive records. Averaging over all defines $T_{2,\phi}^\star$. The correlator σ_B^2 is calculated from the frequency difference between the first and last record (horizontal green arrow). Postselection is performed by averaging over all blocks of records that start in a frequency window $f_0 \pm \Delta f/2$ (upward red arrows), giving for $N = 1$ the red trace in the lower inset defining $T_{2,ps}^\star$. (In this illustration, we neglect the complication of block overlaps that can happen for $N > 1$). Blocks of records defining $T_{2,QC}^\star$ are those of $T_{2,ps}^\star$ shifted by 1 record (downward purple arrows), giving for $N = 1$ the purple trace in the lower inset defining $T_{2,QC}^\star$. (b) Ratios $\overline{T_{2,\phi}^\star}/T_{2,B}^\star$ (black squares) and $T_{2,QC}^\star/T_{2,B}^\star$ (purple triangles). Black dashed line (dotted black line): analytical limit for large N for the mean shape ratio $k = 7.25$ (for $k \in \langle 6, 8.5 \rangle$). Purple dashed line: analytical limit for large N. Purple solid line: numerical evaluation of the integral leading to Eq. (4) [26]. (c) Enhancement of $T_{2,ps}^\star$ (red upwards triangles) and $T_{2,QC}^\star$ (purple downwards triangles) by thresholding on the width of the estimator probability distribution peak. Inset: distribution of estimator probability peak width.

with $k = 4/\gamma_1^2$ given by the skewness γ_1 of the Gamma distribution of $T_{2,\phi}^\star$ and we used $k = 7.5$ to evaluate the ratio. The measured values are shown in Fig. 4(b) as black squares while Eq. (3) is shown by a black dashed line,

showing the expected agreement for $N \gg 1$ with small deviations. Second,

$$\frac{T_{2,QC}^\star}{T_{2,B}^\star} = \sqrt{\frac{1}{2}\left(8\sqrt{2} - 1 - \sqrt{1 + 16\sqrt{2}}\right)} \approx 1.65. \quad (4)$$

The ratio extracted from the measurement is shown in Fig. 4(b) as purple downward triangles. The $N \gg 1$ limit is displayed as a purple dashed line and a straightforward numerical calculation for finite N as a purple solid line, showing excellent agreement with the data.

We can further enhance the qubit coherence by constraining the selected records according to progressively smaller widths of the Bayesian estimator probability distribution. As shown in Fig. 4(c), this boosts $T_{2,QC}^\star$ beyond 1 μs by better estimating the oscillation frequency f_0. Even though similar or even larger values have been reported in GaAs [13] or other materials [29–31], our architecture is explicitly a multiqubit one. The presence of the third spin, which was probably the main limitation of the Bayesian estimator precision [see right inset of Fig. 2(a)] [26], nevertheless, manifestly proves that GaAs provides a robust platform for scalable architectures [32,33] with long coherence times. In addition, the qubit-qubit coupling we see offers resources for quantum computation, e.g., allowing implementation of entangling gates.

We would like to point out that one should be cautious about an apparent enhancement of the phase stability obtained by sophisticated postprocessing. As an example, we can push $T_{2,ps}^\star$ up to 10 μs, using the postselection described in the previous paragraph by which we effectively select records with especially low noise history. With little relevance for practical quantum computation, it nevertheless allows us to move towards the quantum mechanical limit set by T_2, which was argued to be much shorter for a free induction decay (our experiment) than in a Hahn echo sequence [34], where $T_2 \sim 30$ μs has been reported [11]. As we see no apparent saturation of $T_2^\star$ in the postselection despite our sample not being optimized to maximize $T_2^\star$, we believe that the dephasing time will be further increased by straightforwardly reducing the acquisition time. This should allow access to both the quantum mechanical decay of the spin qubit and short-time dynamics of nuclei. Both are open problems with many interesting theoretical predictions which await experimental investigation [20,35,36].

---

[*]matthieu.delbecq@riken.jp

[1] A. Abragam, *The Principles of Nuclear Magnetism* (Oxford University Press, New York, 1961), p. 618.

[2] C. Poole, *Electron Spin Resonance*, 2nd ed. (Wiley, New York, 1993).

[3] D. P. DiVincenzo, Quantum Computation, Science **270**, 255 (1995).

[4] D. Loss and D. P. DiVincenzo, Quantum computation with quantum dots, Phys. Rev. A **57**, 120 (1998).

[5] J. R. Petta, A. C. Johnson, J. M. Taylor, E. A. Laird, A. Yacoby, M. D. Lukin, C. M. Marcus, M. P. Hanson, and A. C. Gossard, Coherent manipulation of coupled electron spins in semiconductor quantum dots, Science **309**, 2180 (2005).

[6] I. A. Merkulov, A. L. Efros, and M. Rosen, Electron spin relaxation by nuclei in semiconductor quantum dots, Phys. Rev. B **65**, 205309 (2002).

[7] A. V. Khaetskii, D. Loss, and L. Glazman, Electron Spin Decoherence in Quantum Dots due to Interaction with Nuclei, Phys. Rev. Lett. **88**, 186802 (2002).

[8] B. Urbaszek, X. Marie, T. Amand, O. Krebs, P. Voisin, P. Maletinsky, A. Högele, and A. Imamoglu, Nuclear spin physics in quantum dots: An optical investigation, Rev. Mod. Phys. **85**, 79 (2013).

[9] D. Paget, G. Lampel, B. Sapoval, and V. I. Safarov, Low field electron-nuclear spin coupling in gallium arsenide under optical pumping conditions, Phys. Rev. B **15**, 5780 (1977).

[10] P. Maletinsky, A. Badolato, and A. Imamoglu, Dynamics of Quantum Dot Nuclear Spin Polarization Controlled by a Single Electron, Phys. Rev. Lett. **99**, 056804 (2007).

[11] H. Bluhm, S. Foletti, I. Neder, M. Rudner, D. Mahalu, V. Umansky, and A. Yacoby, Dephasing time of GaAs electron-spin qubits coupled to a nuclear bath exceeding 200 μs, Nat. Phys. **7**, 109 (2011).

[12] R. de Sousa, Electron Spin as a Spectrometer of Nuclear-Spin Noise and Other Fluctuations, Top. Appl. Phys. **115**, 183 (2009).

[13] M. D. Shulman, S. P. Harvey, J. M. Nichol, S. D. Bartlett, A. C. Doherty, V. Umansky, and A. Yacoby, Suppressing qubit dephasing using real-time Hamiltonian estimation, Nat. Commun. **5**, 5156 (2014).

[14] M. Pioro-Ladrière, T. Obata, Y. Tokura, Y.-S. Shin, T. Kubo, K. Yoshida, T. Taniyama, and S. Tarucha, Electrically

[15] R. Hanson, L. P. Kouwenhoven, J. R. Petta, S. Tarucha, and L. M. K. Vandersypen, Spins in few-electron quantum dots, Rev. Mod. Phys. **79**, 1217 (2007).

[16] C. Barthel, J. Medford, H. Bluhm, A. Yacoby, C. M. Marcus, M. P. Hanson, and A. C. Gossard, Relaxation and readout visibility of a singlet-triplet qubit in an Overhauser field gradient, Phys. Rev. B **85**, 035306 (2012).

[17] A. Sergeevich, A. Chandran, J. Combes, S. D. Bartlett, and H. M. Wiseman, Characterization of a qubit Hamiltonian using adaptive measurements in a fixed basis, Phys. Rev. A **84**, 052315 (2011).

[18] M. C. Wang and G. E. Uhlenbeck, On the Theory of the Brownian Motion II, Rev. Mod. Phys. **17**, 323 (1945).

[19] A. G. Redfield, Spatial Diffusion of Spin Energy, Phys. Rev. **116**, 315 (1959).

[20] D. Klauser, W. A. Coish, and D. Loss, Nuclear spin dynamics and Zeno effect in quantum dots and defect centers, Phys. Rev. B **78**, 205301 (2008).

[21] J.-P. Bouchaud and A. Georges, Anomalous diffusion in disordered media: Statistical mechanisms, models and physical applications, Phys. Rep. **195**, 127 (1990).

[22] R. Metzler and J. Klafter, The random walk's guide to anomalous diffusion: a fractional dynamics approach, Phys. Rep. **339**, 1 (2000).

[23] Y. Li, N. Sinitsyn, D. L. Smith, D. Reuter, A. D. Wieck, D. R. Yakovlev, M. Bayer, and S. A. Crooker, Intrinsic Spin Fluctuations Reveal the Dynamical Response Function of Holes Coupled to Nuclear Spin Baths in (In,Ga)As Quantum Dots, Phys. Rev. Lett. **108**, 186603 (2012).

[24] D. J. Reilly, J. M. Taylor, E. A. Laird, J. R. Petta, C. M. Marcus, M. P. Hanson, and A. C. Gossard, Measurement of Temporal Correlations of the Overhauser Field in a Double Quantum Dot, Phys. Rev. Lett. **101**, 236803 (2008).

[25] J. Medford, L. Cywiski, C. Barthel, C. M. Marcus, M. P. Hanson, and A. C. Gossard, Scaling of Dynamical Decoupling for Spin Qubits, Phys. Rev. Lett. **108**, 086802 (2012).

[26] See Supplemental Material at http://link.aps.org/supplemental/10.1103/PhysRevLett.116.046802 for details about data analysis and theoretical derivations of the various $T_2^\star$.

[27] E. Hahn, Spin Echoes, Phys. Rev. **80**, 580 (1950).

[28] L. M. K. Vandersypen and I. L. Chuang, NMR techniques for quantum control and computation, Rev. Mod. Phys. **76**, 1037 (2005).

[29] B. M. Maune, M. G. Borselli, B. Huang, T. D. Ladd, P. W. Deelman, K. S. Holabird, A. A. Kiselev, I. Alvarado-Rodriguez, R. S. Ross, A. E. Schmitz, M. Sokolich, C. A. Watson, M. F. Gyure, and A. T. Hunter, Coherent singlet-triplet oscillations in a silicon-based double quantum dot, Nature (London) **481**, 344 (2012).

[30] E. Kawakami, P. Scarlino, D. R. Ward, F. R. Braakman, D. E. Savage, M. G. Lagally, M. Friesen, S. N. Coppersmith, M. A. Eriksson, and L. M. K. Vandersypen, Electrical control of a long-lived spin qubit in a Si/SiGe quantum dot, Nat. Nanotechnol. **9**, 666 (2014).

[31] M. Veldhorst, J. C. C. Hwang, C. H. Yang, A. W. Leenstra, B. de Ronde, J. P. Dehollain, J. T. Muhonen, F. E. Hudson,

K. M. Itoh, A. Morello, and A. S. Dzurak, An addressable quantum dot qubit with fault-tolerant control-fidelity, Nat. Nanotechnol. **9**, 981 (2014).

[32] M. R. Delbecq, T. Nakajima, T. Otsuka, S. Amaha, J. D. Watson, M. J. Manfra, and S. Tarucha, Full control of quadruple quantum dot circuit charge states in the single electron regime, Appl. Phys. Lett. **104**, 183111 (2014).

[33] T. Otsuka, T. Nakajima, M. R. Delbecq, S. Amaha, J. Yoneda, K. Takeda, G. Allison, T. Ito, R. Sugawara, A. Noiri, A. Ludwig, A. D. Wieck, and S. Tarucha,

Single-electron Spin Resonance in a Quadruple Quantum Dot, arXiv:1510.02547.

[34] W. Yao, R.-B. Liu, and L. J. Sham, Theory of electron spin decoherence by interacting nuclear spins in a quantum dot, Phys. Rev. B **74**, 195301 (2006).

[35] W. A. Coish and D. Loss, Hyperfine interaction in a quantum dot: Non-Markovian electron spin dynamics, Phys. Rev. B **70**, 195340 (2004).

[36] C. Deng and X. Hu, Analytical solution of electron spin decoherence through hyperfine interaction in a quantum dot, Phys. Rev. B **73**, 241303 (2006).